Analysis Note: The Proton-Ω Correlation Function

(Dated: December 2, 2017)

INTRODUCTION

Exotic particles, with quark content different from conventional hadrons, have been proposed long ago [1].The Nucleon-Ω ($N\Omega$) state with the strangeness = -3, spin = 2 and isospin = 1/2 is the most interesting candidate [2–6] after H-dibaryon. Similar to H-dibaryon the Pauli exclusion principle does not apply among quarks in the $N\Omega$ dibaryon and it is stable against strong decay [7, 8]. Several attempts are made to estimate the binding energy of the $N\Omega$ state in different QCD motivated models [9, 10]. For a S-wave bound state of nucleon and Ω, the strong decays to octet-decuplet systems are prohibited by kinematics and those into octet-octet systems (e.g. ΛΞ) are suppressed dynamically due to the D-wave nature [10].

Using the proton-Ω interaction extracted from (2+1)-flavor lattice QCD simulations, in Ref [11] authors showed that the two particle correlation function changes substantially with the strength of the proton-Ω attraction. However the presence of the Coulomb interaction in the proton-Ω channel makes it difficult to access strong interaction directly from the measured two particle correlation function. Therefore, a new measure - the ratio of the correlation function between the small and large collision systems is proposed in Ref [11]. This ratio provides direct access to strong interaction for proton-Ω and is not sensitive to the model used for emission source. We measure the proton-Ω correlation function for central (0-40%) and peripheral (40-80%) collisions for Au+Au at $\sqrt{s_{NN}}$ = 200 GeV . Using these we measure the ratio of the proton-Ω correlation function in peripheral to central collisions for Au+Au at $\sqrt{s_{NN}}$ = 200 GeV.

ANALYSIS DETAILS

DATA Selection

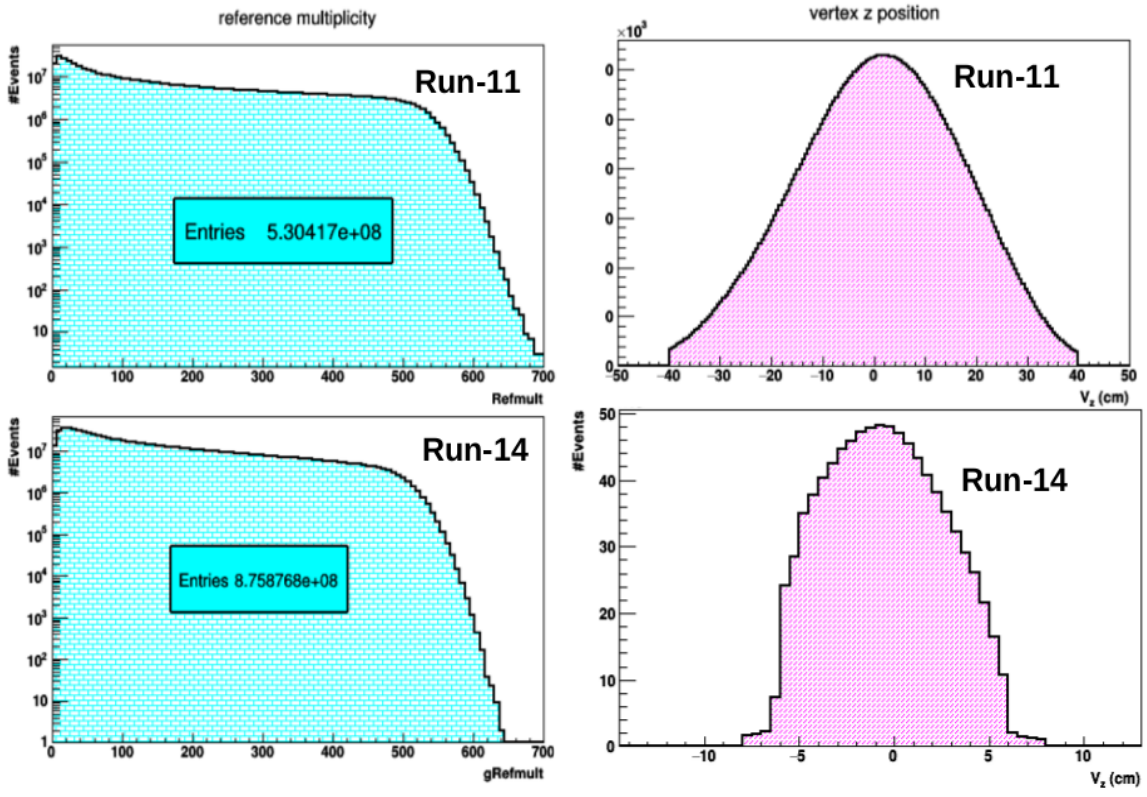

FIG. 1. Reference multiplicity distribution of selected events for run-11 and run-14 are shown in left panels and z-vertex distribution of selected events for run-11 and run-14 are shown in right panels.

The data taken for Au+Au collisions at $\sqrt{s_{NN}}$=200 GeV in 2011 and 2014 with approximately 5.30×10^8 minimum bias events from 2011 and 8.76×10^8 minimum bias events from 2014 were analyzed. The tracking and particle

identification for the measurements were provided by the Time Projection Chamber (TPC) and Time-of-Flight (TOF) detectors. Minimum bias triggered events were selected by requiring coincident signals at forward and backward rapidities in the Vertex Position Detectors (VPD) with a signal at mid-rapidity in the TOF. Centrality was determined by the charged particle multiplicity at mid-rapidity in the TPC using the standard star RefMult defination for 2011 and gRefMult for 2014 data. To analyze data nine Centrality bins: 0-5, 5-10, 10-20, 20-30, 30-40, 40-50, 50-60, 60-70 and 70-80 were used. Then results from different centralities were combined to get final results for 0-40% and 40-80% centralities. To suppress events from collisions with the beam pipe, the reconstructed primary vertex was required to lie within a 2 cm radial distance from the center of the beam pipe. In addition, the z-position of the vertex was required to lie within ± 40 (± 6) cm of the center of the detector for the data from 2011 (2014). Also following track quality cuts were used:

- Number of fit points > 15
- Ratio of fit points to possible points > 0.52
- p_T cut for proton and pion tracks > 0.15 GeV/c

The reference multiplicity distribution and z-vertex are shown in Figure 1.

Ω IDENTIFICATION

Selection criteria	0-40%		40-80%
	$p_T < 2.5$ GeV/c	$p_T > 2.5$ GeV/c	All p_T
Ω DCA	< 0.6 cm	< 0.7 cm	< 0.8 cm
Λ DCA	> 0.4 cm	> 0.3 cm	> 0.3 cm
DL(Ω)	> 4.0 cm	> 4.0 cm	> 3.0 cm
DL(Λ)	> 6.0 cm	> 6.0 cm	> 5.0 cm
$\lvert(R_\Omega - R_{PV}) \times p_\Omega\rvert / \lvert R_\Omega - R_{PV}\rvert\lvert p_\Omega\rvert$	< 0.05	< 0.08	< 0.15
$DL(\Omega) < DL(\Lambda)$	Yes	Yes	Yes
proton DCA	> 0.8 cm	> 0.8 cm	> 0.6 cm
pion DCA	> 2.0 cm	> 2.0 cm	> 1.8 cm
bachlor DCA	> 1.2 cm	> 1.2 cm	> 1.0 cm
proton to pion DCA	< 0.8 cm	< 0.8 cm	< 1.0 cm
Λ DCA to bachlor	< 0.8cm	< 0.8cm	< 1.0cm
nσ(proton)	< 3	< 3	< 3
nσ(pion)	< 3	< 3	< 3
nσ(bachlor)	< 3	< 3	< 3
$\lvert IM_\Lambda - 1.1156\rvert$	$< 7MeV/c^2$	$< 7MeV/c^2$	$< 7MeV/c^2$
$\lvert IM_\Omega - 1.672\rvert$	$< 7MeV/c^2$	$< 7MeV/c^2$	$< 7MeV/c^2$

TABLE I. Selection cuts for Ω and $\bar{\Omega}$.

The TPC was used for tracking and particle identification for Ω ($\bar{\Omega}$) reconstruction in the pseudo-rapidity range $|\eta| < 1$. To reconstruct the Ω ($\bar{\Omega}$), the decay channel $\Omega(\bar{\Omega}) \rightarrow \Lambda K^-(\bar{\Lambda}K^+)$, with a branching ratio - 67.8%, with subsequent decay to $\Lambda(\bar{\Lambda}) \rightarrow p\pi^-(\bar{p}\pi^+)$ (branching ratio - 63.9%) was used [13]. The Λ ($\bar{\Lambda}$) candidates were formed from pairs of p ($\bar{p}$) and π^- (π^+) tracks whose trajectories pointed to a common secondary decay vertex which was well separated from the Ω ($\bar{\Omega}$) vertex. These Λ ($\bar{\Lambda}$) candidates were then combined with bachelor K^- (K^+) tracks which points to a common decay vertex well separated from the primary vertex. Selection cuts on decay length of Ω and Λ, distance of closest approach (DCA) between the two Λ ($\bar{\Lambda}$) daughter tracks, between Λ ($\bar{\Lambda}$) and bachelor track, the Λ ($\bar{\Lambda}$) and the primary vertex position and Ω ($\bar{\Omega}$) candidate pointing angle with respect to the primary vertex were applied to select Ω ($\bar{\Omega}$). All these cuts are listed in Table I, where DCA is distance of closest approach, DL(Ω) is decay length of Ω and DL(Λ) is decay length of Λ. To reduce the combinatorial background, Λ ($\bar{\Lambda}$) candidates were selected in the invariant mass range between 1.112 and 1.120 GeV/c^2. In addition, the candidates due to misidentification of π^- (π^+) tracks as the bachelor K^- (K^+) tracks were removed by checking Ξ hypothesis. The candidates satisfying Ξ hypothesis were removed by applying a cut on reconstructed Invariant mass $|IM - 1.321|$ with misidentified bachelor tracks to be greater than 0.015 GeV/c^2. The effect of this cut is shown in figure 2. The invariant mass distribution of

combined Ω and $\bar{\Omega}$ candidates in different transverse momentum p_T bins are shown in Figure 3 for 0-40% centrality and in Figure 4 for 40-80% centrality.

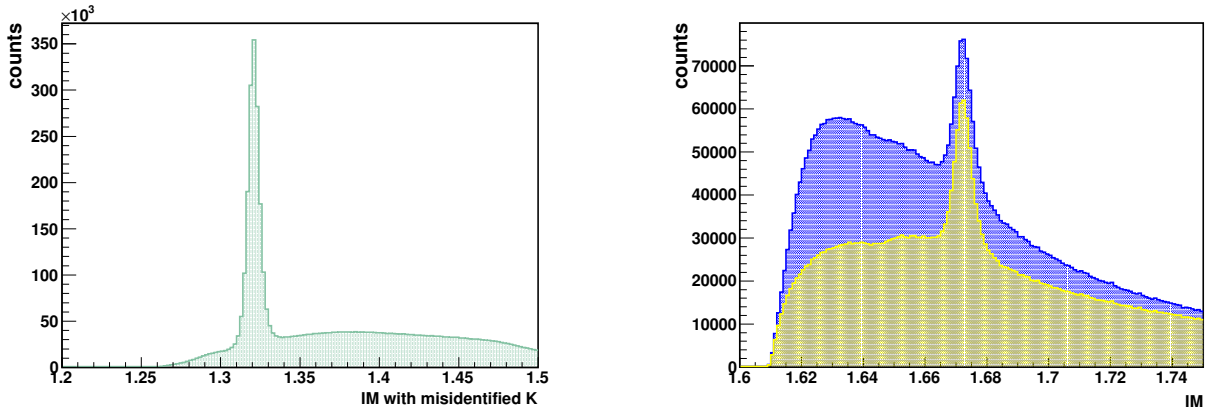

FIG. 2. Removal of Ξ candidates deu to misidentification of kaons. The left figure shows reconstructed invariant mass with misidenfied pions as kaons in our analysis. Candidates within 3σ of Ξ mass are removed from the analysis. The right figure shows the reconstructed Ω invariant mass after removing candidates which satisfy the Ξ hypothesis. Blue histogram before removal of candidates satisfying the Ξ hypothesis and yellow is after removal.

Purity, P(Ω) is calculated as the ratio of S to (S+B) for Ω in each p_T bins, where S is signal and B is background. To extract Ω signal count, the invariant mass distribution of Ω in each p_T bins are fitted with Gaussian+polynomial function. Figure 5 shows one such fit for the p_T range (2.0,2.5) GeV/c for 0-40% centrality. Then the purity of the Ω is calculated by taking the ratio of S to (S+B) and is plotted in Figure 6.

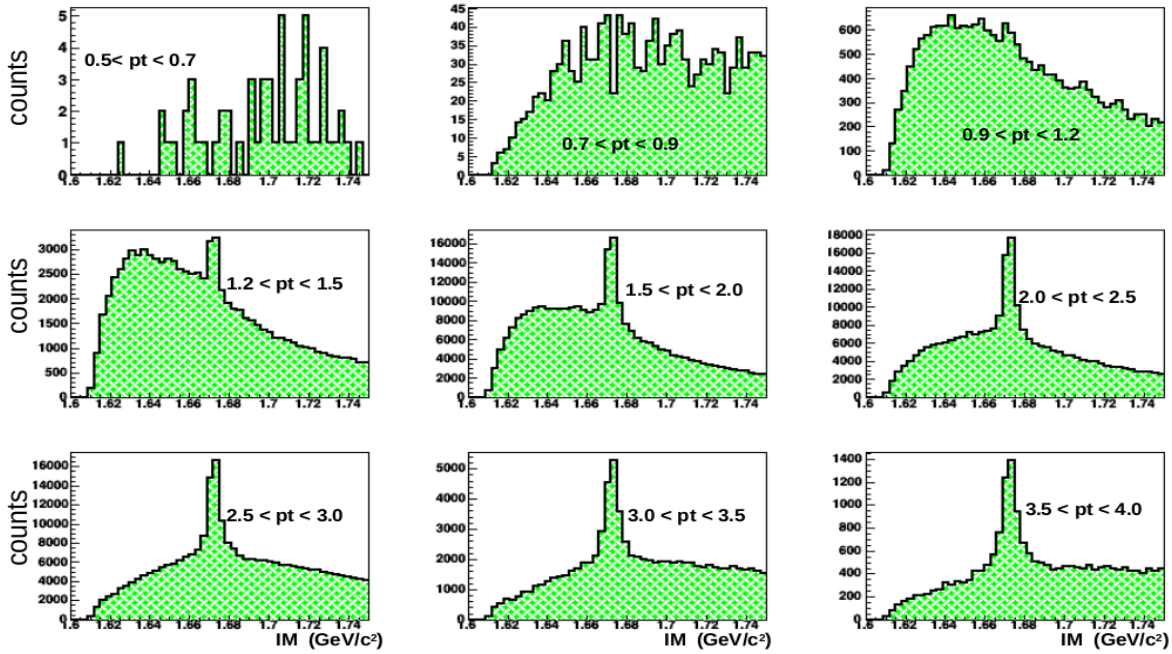

FIG. 3. Reconstructed invariant mass of combined Ω and $\bar{\Omega}$ sample for 0-40% for all p_T bins.

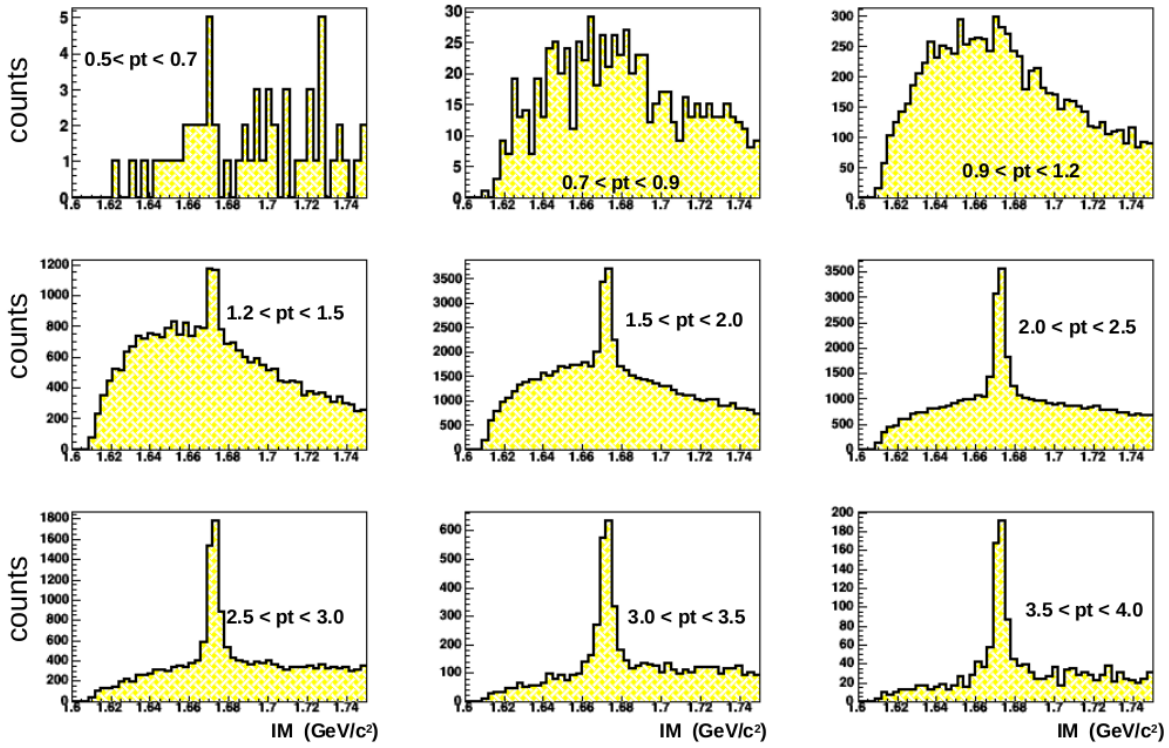

FIG. 4. Reconstructed invariant mass of combined Ω and $\bar{\Omega}$ sample for 40-80% for all p_T bins.

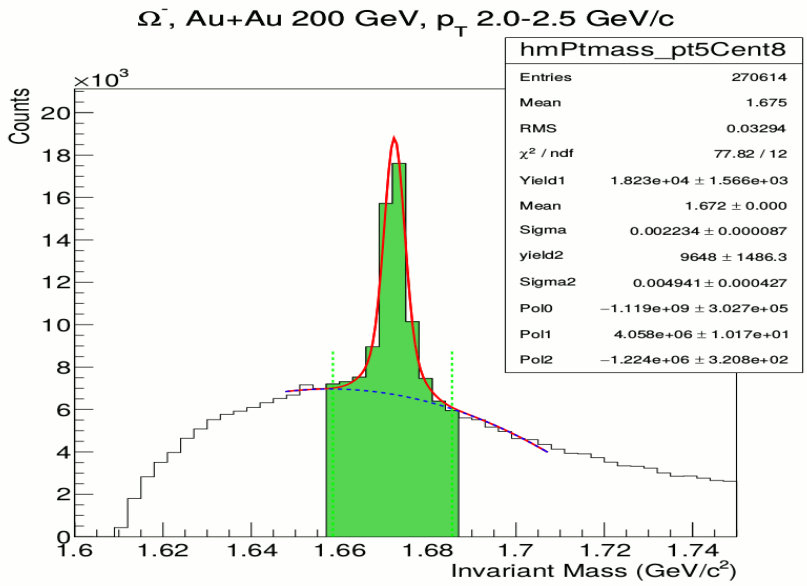

FIG. 5. Fit to the reconstructed invariant mass of Ω for the p_T range (2.0-2.5) GeV/c in 0-40% centrality.

PROTON IDENTIFICATION

The TOF and TPC detectors were used for proton (anti-proton) identification in the pseudo-rapidity range $|\eta| < 1$. The proton tracks were selected if their DCA was less than 0.5 cm from the primary vertex, greater than 20 points measured in the TPC out of a maximum of 45 and the number of points used in track reconstruction divided by the number of possible points was greater than 0.52 in order to prevent split tracks. The time of flight of particles reaching

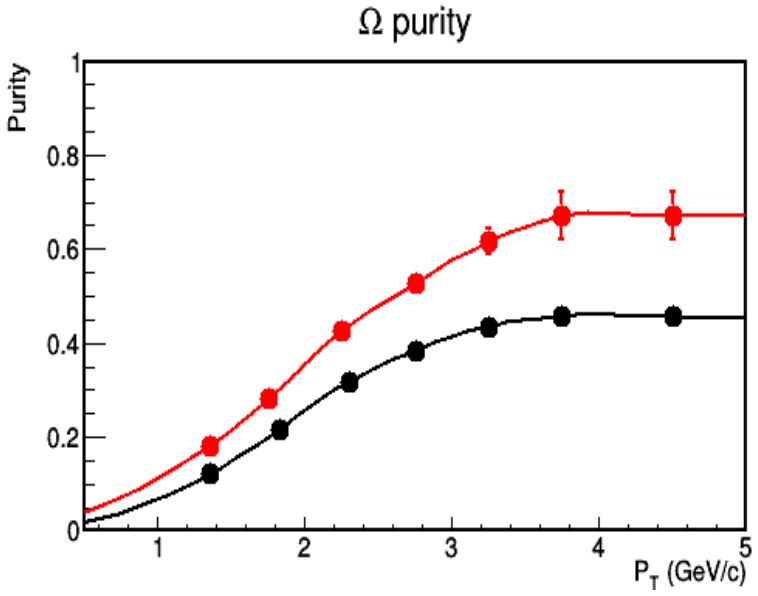

FIG. 6. Purity of the Ω sample in 0-40% (black circle) and 40-80% (red circle) as a function of p_T.

the TOF detector along with the tracking information from the TPC detector was used to derive the square of the particle mass (m^2) to identify protons. Figure 7 shows one such particle identification using m^2 from TOF detector versus momentum from the TPC detector. All candidates with m^2 between 0.75 and 1.10 $(\mathrm{GeV}/c^2)^2$ were considered for further measurement. To obtain the proton purity, P(p), the m^2 distribution is fitted with three Gaussian function as shown in Figure 8 and the obtained purity (S/(S+B)) is plotted in Figure 9.

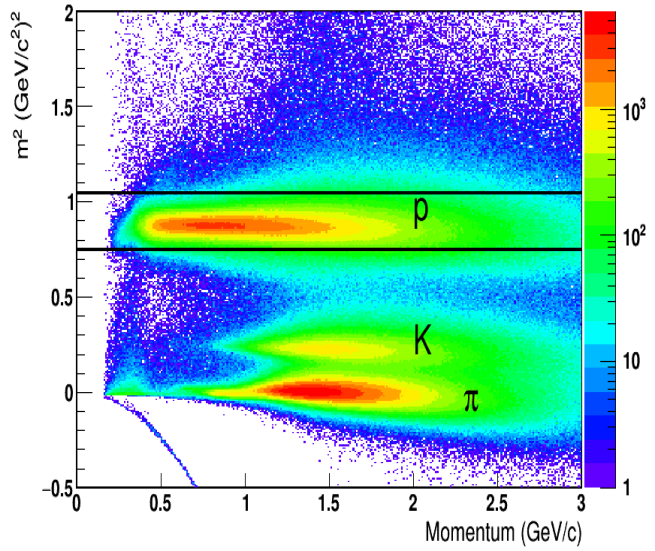

FIG. 7. Proton identification using the time of flight from TOF detector and momentum from the TPC detector. The solid lines show the reconstructed proton candidates used for the measurement of proton-Ω correlation function.

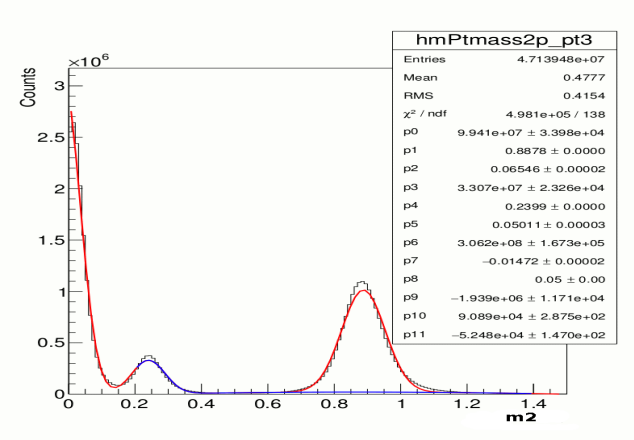

FIG. 8. Fit to m^2 distribution in p_T range (1.2-1.5) GeV/c.

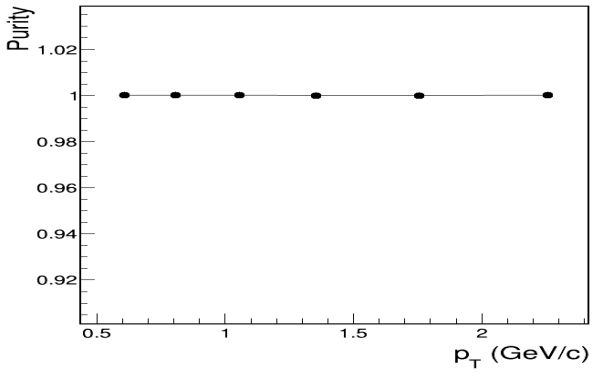

FIG. 9. Purity of the proton sample as a function of p_T.

TWO PARTICLE CORRELATION FUNCTION

The two-particle correlation function is defined as

$$C_{\text{measured}}(k^*) = \frac{A(k^*)}{B(k^*)}, \tag{1}$$

where $A(k^*)$ is the distribution of the invariant relative momentum, k^*, for a pair of proton and Ω, anti-proton and $\bar{\Omega}$ from the same event. $B(k^*)$ is the reference distribution generated by mixing particles from different events. For mixed events, the selected events are required to have same bin in centrality and event vertex position. The z-vertex binning of 10 cm (2 cm) is used for 2011 (2014) data. The same single-particle cuts were applied to individual proton (anti-proton) and Ω ($\bar{\Omega}$) for the mixed-event pairs. Since the track selection for reconstruction of Ω and primary protons involve different track selection criteria, like selection of tracks with unique track id for daughter protons and primary protons and cut on distance of closest approach of primary proton is < 0.5 cm, where as for daughter protons the cut on DCA is > 0.8 cm, the contribution from effects like track splitting and track merging is negligible to measured correlation function. The efficiency and acceptance effects canceled out in the ratio $A(k^*)/B(k^*)$. However one needs to correct the measured correlation function for the purity of the Ω and proton samples used in the analysis. Corrections to the raw correlation functions for pair purity were applied according to the expression

$$C'(k^*) = \frac{C_{\text{measured}}(k^*) - 1}{P(k^*)} + 1, \tag{2}$$

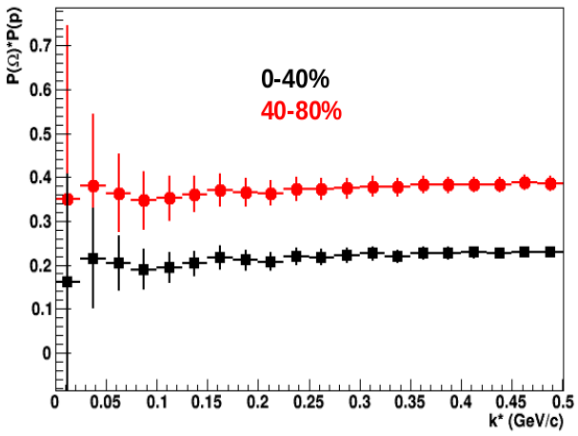

FIG. 10. Pair purity of proton-Ω as a function of k^* for 0-40% (black) and 40-80% (red) centrality.

where the pair purity, $P(k^*)$, was calculated as a product of $S/(S+B)$ for the Ω and purity of the proton. The selected sample of proton candidates also included secondary protons from Λ, Σ and Ξ. The estimated fraction of primary protons (anti-protons) from Thermal model [14] studies are F(k*) = 52% (48%), these esitmates are taken from the Published STAR paper on proton-Λ correlation function [15]. While estimating fraction of primaries, no detector geometry/material is used. Therefore same fraction is used for both 2011 and 2014 data set. The purity of the proton sample, P(p), is obtained as a product of identification probability S/(S+B) and fraction of primary protons F(k*) . The pair purity of proton-Ω for 0-40% and 40-80% centrality is shown in Figure 10 and is constant over the analyzed range of invariant relative momentum.

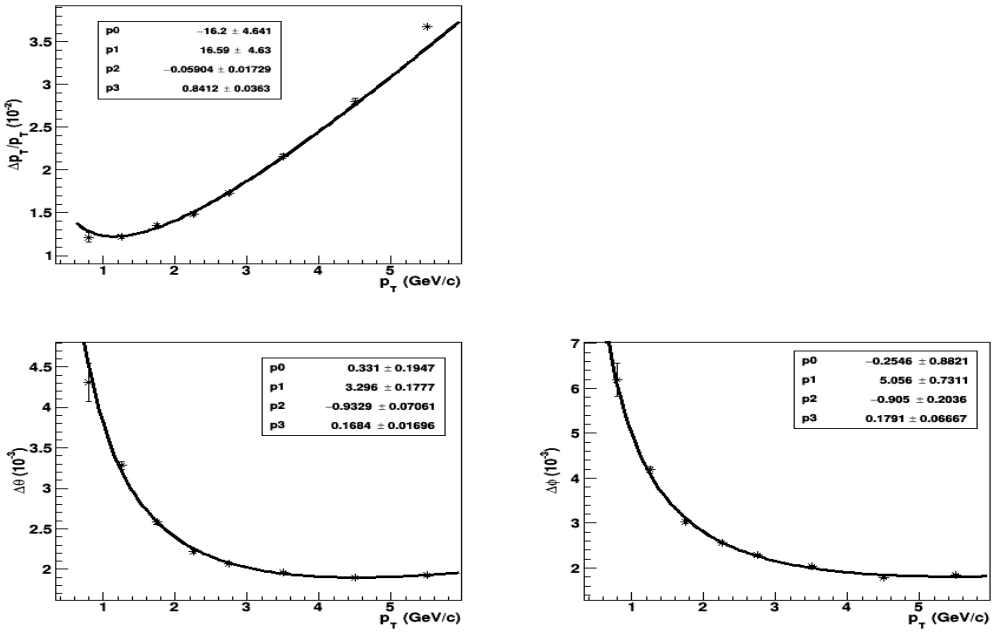

FIG. 11. Smearing factors $\sigma(\Delta p_T/p_T)$,$\sigma(\Delta\phi)$ and $\sigma(\Delta\theta)$ for Ω.

The effect of momentum resolution on the correlation functions has also been investigated using simulated tracks from Ω decay and tracks for protons, with known momenta, embedded into real events. To study this effect, embedding sample of proton with SL15c and Ω with SL11d for Au+Au 200 GeV were used. The flat pt distribution is generated and embedded into the real event. The smearing factors $\sigma(\Delta p_T/p_T)$,$\sigma(\Delta\phi)$ and $\sigma(\Delta\theta)$ are determined by comparing real tracks and embedded tracks. The obtained $\sigma(\Delta p_T/p_T)$, $\sigma(\Delta\phi)$ and $\sigma(\Delta\theta)$ as a function of p_T are shown in

Figure 11 for Ω and in Figure 12 for protons. The distributions are fitted by following function

$$p_0 + p_1 X^{p_2} + p_3 X \tag{3}$$

The values of fit parameters are $p_0, p_1, p_2 and p_3$ listed in the figures. Using these we modify the momentum of proton and Ω to estimate the effect of smearing.

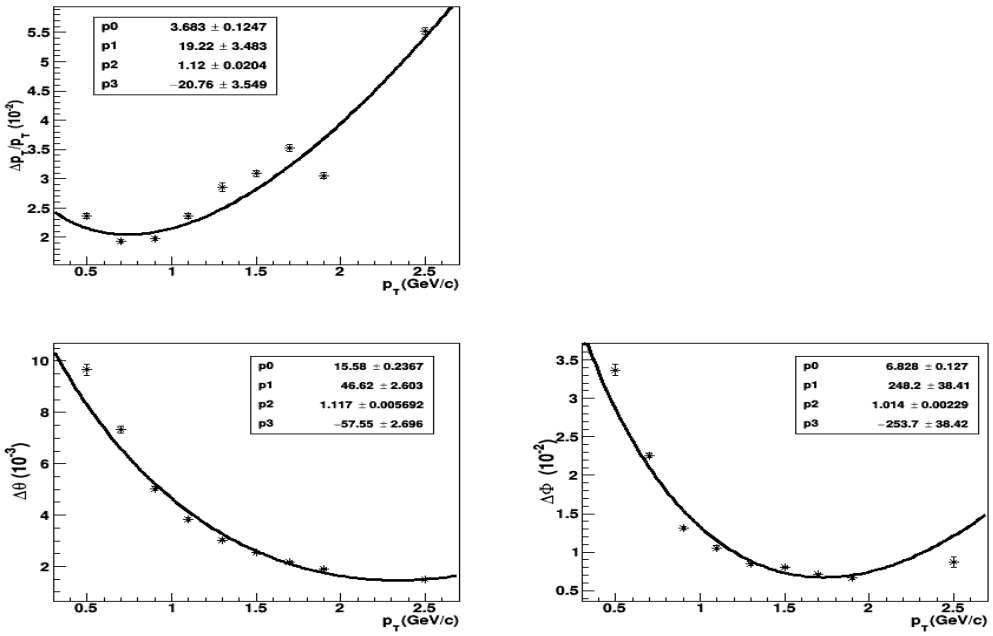

FIG. 12. Smearing factors $\sigma(\Delta p_T/p_T)$,$\sigma(\Delta\phi)$ and $\sigma(\Delta\theta)$ for proton.

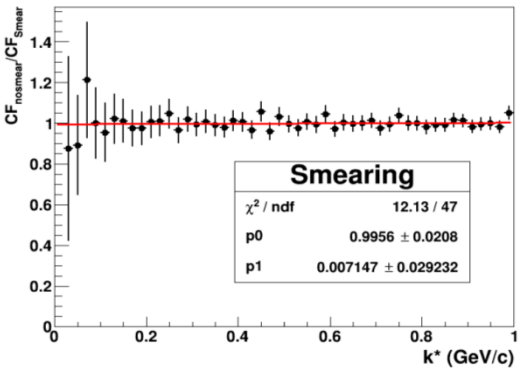

FIG. 13. smearing correction factor $C_{nosmear}(k^*)/C_{smear}(k^*)$. Thr red line is $p_0 + p_1 X$ fit.

Correlation functions have been corrected for momentum resolution using the expression

$$C(k^*) = \frac{C'(k^*) C_{nosmear}(k^*)}{C_{smear}(k^*)}, \tag{4}$$

where $C(k^*)$ represents the corrected correlation function, and $C_{\rm in}(k^*)/C_{\rm res}(k^*)$ is the correction factor. $C_{nosmear}(k^*)$ was calculated without taking into account the effect of momentum resolution and $C_{smear}(k^*)$ included the effect of momentum resolution applied to each Ω and proton candidate. The smearing correction factor $C_{nosmear}(k^*)/C_{smear}(k^*)$ as a function of k^* is shown in Figure 13. The ratio is fitted with $p_0 + p_1 X$. The impact of momentum resolution on correlation functions is negligible ($p_0 = 0.995 \pm 0.021$) compared with statistical errors.

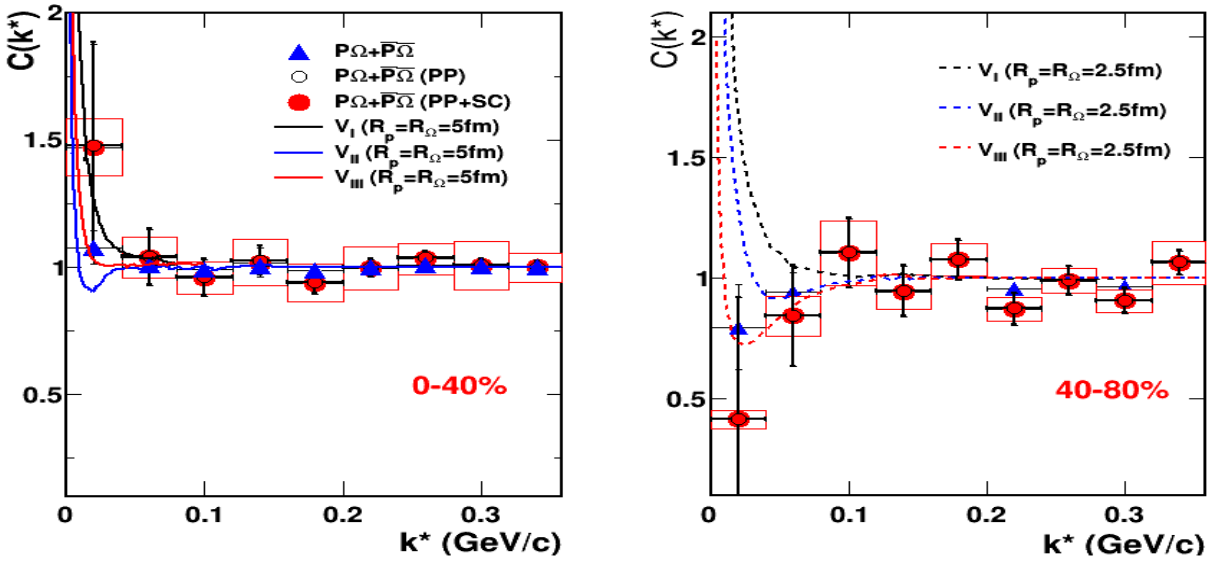

FIG. 14. (color online) Measured correlation function (C(k^*)) for proton-Ω and anti-proton-$\bar{\Omega}$ ($P\Omega + \bar{P}\bar{\Omega}$) in 0-40% (left) and 40-80% (right) Au+Au collisions at $\sqrt{s_{NN}}$=200 GeV. The traingles are raw correlations, open circles are pairpurity corrected (PP) correlations and solid circles are pairpurity and smearing corrected (PP+SC) correlations. The boxes correspond to the systematic errors. The solid and dashed lines are prediction from [11] for proton-Ω interaction potentials V_I, V_{II} and V_{III} for source sizes $R_p = R_\Omega = 5$ fm and $R_p = R_\Omega = 2.5$ fm.

Figure 14 shows the measured proton-Ω and anti-proton-$\bar{\Omega}$ correlation function, $P\Omega + \bar{P}\bar{\Omega}$, correlation function after corrections for pair purity, $P\Omega + \bar{P}\bar{\Omega}$ (PP), and correlation function after corrections for pair purity and momentum smearing, $P\Omega + \bar{P}\bar{\Omega}$ (PP+SC), for 0-40% and 40-80% Au+Au collisions at $\sqrt{s_{NN}}$ = 200 GeV. The predictions of proton-Ω correlation function from [11] for proton-Ω interaction potentials V_I, V_{II} and V_{III} for source sizes $R_p = R_\Omega$ = 2.5 fm and $R_p = R_\Omega$ = 5.0 fm are also shown in figure 14. Binding energy (E_b), scattering length (a_0) and effective range (r_{eff}) used in different proton-Ω interaction potentials V_I, V_{II} and V_{III} are listed in Table II.

Spin-2 pΩ potentials	V_I	V_{II}	V_{III}
E_b (MeV)	-	6.3	26.9
a_0 (fm)	-1.12	5.79	1.29
r_{eff} (fm)	1.16	0.96	0.65

TABLE II. Binding energy (E_b), scattering length (a_0) and effective range (r_{eff}) for the Spin-2 pΩ potentials.

The correlation function for the background is studied by selecting Ω candidates from the sideband region. In our analysis we select Ω candidates within 0.007 GeV/c^2 window around the Ω invariant mass 1.672 GeV/c^2. So for background study we select candidates with the invariant mass < 1.665 GeV/c^2 and > 1.679 GeV/c^2, as shown in the Figure 15. The reconstructed proton-Ω correlation function along with the correlation function for the background for 0-40% and 40-80% centrality are shown in Figure 16. We can observe that the correlation function for the background has similar trend and approximately same amplitude for the lower k^* values for 0-40% and 40-80% centrality.

The systematic uncertainty on the measured proton-Ω correlation function were estimated by varying the selection cuts for Ω and protons around the analysis cuts. For the selection of Ω candidates, the pointing angle cuts (sin(θ)) and mass range which affect the purity of the Ω sample, were varied to estimate systematic uncertainty on correlation function. The DCA and m^2 requirements were varied to estimate systematic from the proton purity. In addition systematic from normalization and feed-down contributions were also estimated. The details of the cuts are listed in Table III. Then the relative error is estimated by looking at $\Delta C = C_{var} - C_{ana}/C_{ana}$, where C_{var} is the correlation function with change in the cut and C_{ana} is the correlation function with the cuts used for measurement. These

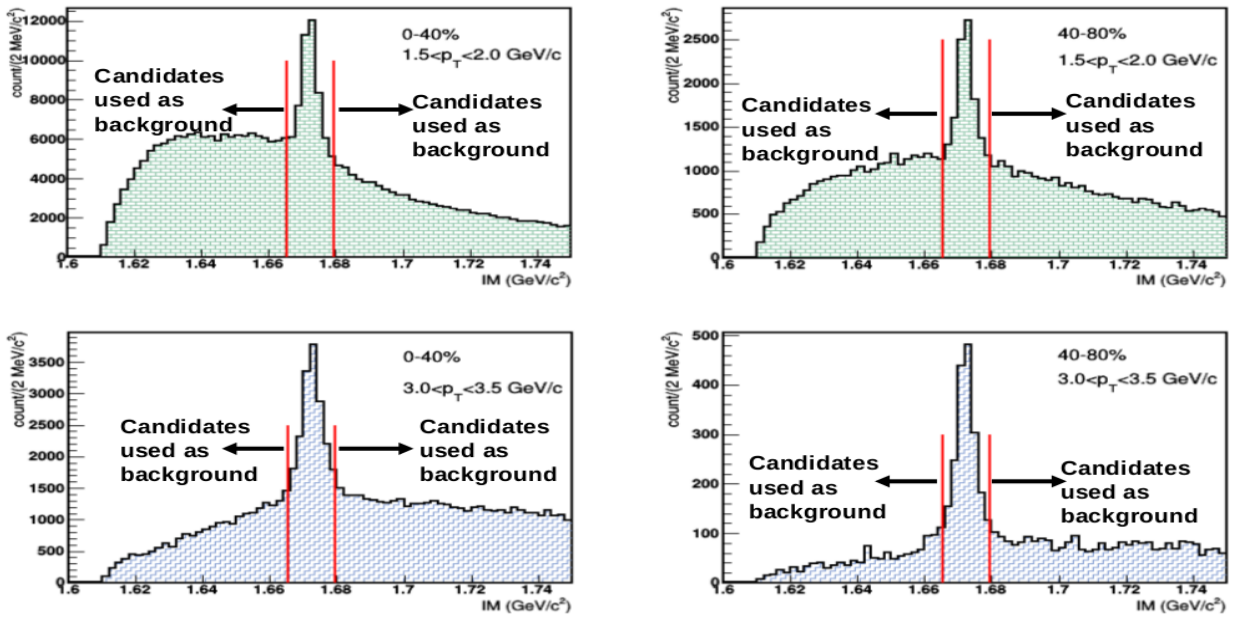

FIG. 15. Selection of candidates for background study.

uncertainties for different sources are shown in Figure 17. To get final systematics on the correlation function for 0-40% and 40-80% centrality, the uncertainties from different sources were added in quadrature as shown by Figure 18.

Note that the uncertainty on first two bins in Figure 17 and Figure 18 are very large compared to uncertainty on the higher k^* bins. This is due to statistical fluctuations in those bins. The number of proton-Ω pairs in those two bins are very small and the statistical fluctuation introduces larger deviation in correlation function for the change in cuts than the measured correlation. This is clearly visible if one compares the systematics from 0-40% and 40-80% centrality. In 40-80% centrality the proton-Ω pairs are order of magnitude small at low k^* bins (Figure 19) and we estimate

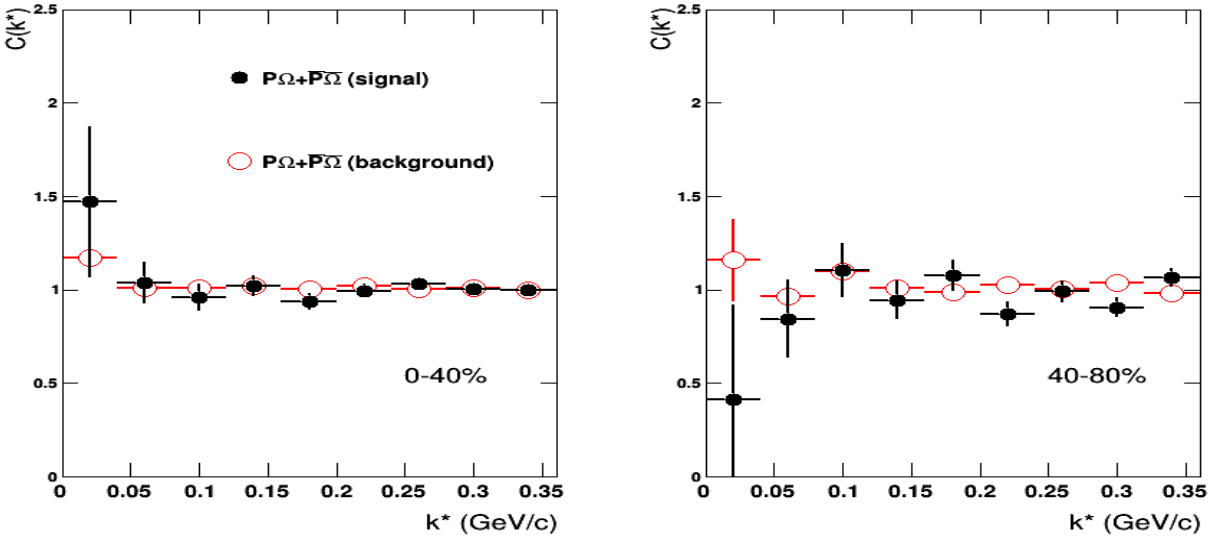

FIG. 16. Proton-Ω correlation function (black circles) for 0-40% (left) and 40-80% (right) are shown along with the background (open red circles), where candidates for background are selected outside the signal region, with IM $<$ 1.665 and IM $>$ 1.679 GeV/c2.

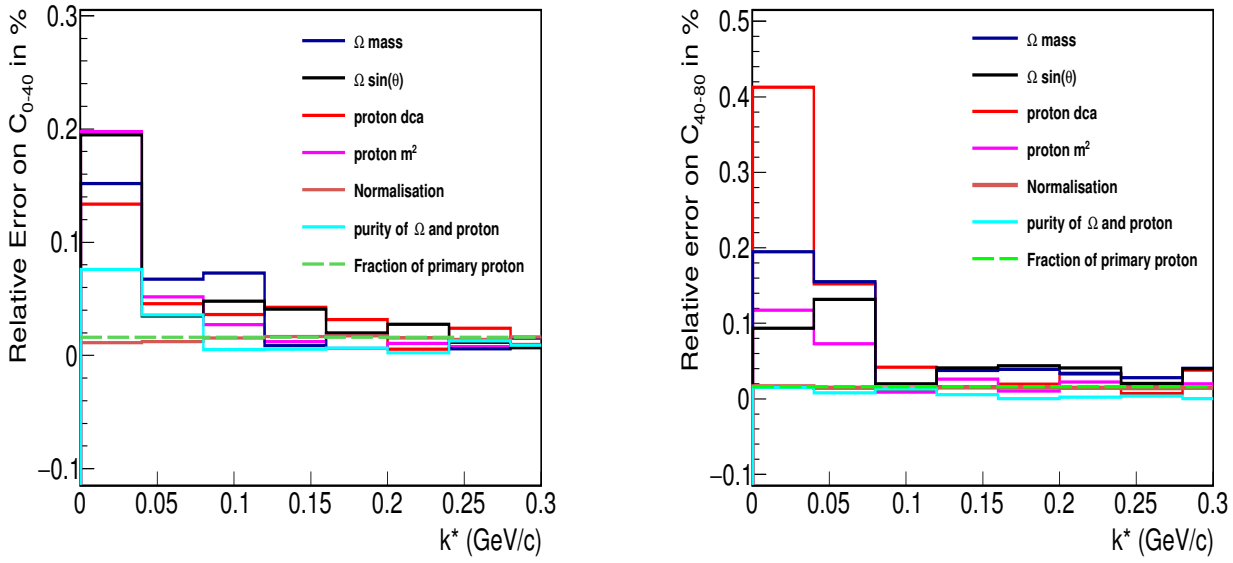

FIG. 17. Esitmated relative errors on correlation function from different sources for 0-40% (left) and 40-80% (right) centrality.

Selection criteria	cuts used for measurement	cuts for sys. estimation	
$\lvert IM_\Omega - 1.672\rvert$	$< 0.007 GeV/c^2$	$< 0.005 GeV/c^2$	$< 0.009 GeV/c^2$
$\lvert(R_\Omega - R_{PV}) \times p_\Omega\rvert/\lvert R_\Omega - R_{PV}\rvert\lvert p_\Omega\rvert$ $(p_T < 2.5, 0-40\%)$	< 0.05	< 0.04	< 0.06
$\lvert(R_\Omega - R_{PV}) \times p_\Omega\rvert/\lvert R_\Omega - R_{PV}\rvert\lvert p_\Omega\rvert$ $(p_T > 2.5, 0-40\%)$	< 0.08	< 0.07	< 0.09
$\lvert(R_\Omega - R_{PV}) \times p_\Omega\rvert/\lvert R_\Omega - R_{PV}\rvert\lvert p_\Omega\rvert$ $(40-80\%)$	< 0.15	< 0.14	< 0.16
Primary proton DCA	< 0.5 cm	< 0.4 cm	< 0.6 cm
Rapidity	1.0	0.5	0.7
k^* range for normalization	0.3-1 GeV/c	0.3-0.7 GeV/c	0.3-1.3 GeV/c
F(k^*)	0.52	0.48	0.56

TABLE III. Variation of cuts for estimation of systematic uncertainty.

larger systematics here. In order to avoid overestimation of systematic uncertainty due to statistical fluctuation, we used two approaches. In the first approach, we combine the first two bins to estimate systematics uncertainty. The systematic uncertainty before and after rebinning are shown in figure 20(left). In the second approach, we estimated the sytematics by taking the average of systematics in all the bins as shown in figure 20 (left). One can see that the estimated error for 0-40% from both the methods, rebinning (5.29%)and average (7.72%), are roughly same for the first two bins. Whereas the systematics for 40-80% from the rebinning method (28.86%) is roughly thrice than the average method (9.56%), which is due the dominance of statitical flutuations in the first two bins. Therefore instead of assigning overestimated errors from rebinning method, we use average over all the bins as final systematic uncertainties, which are shown as boxes in Figure 14. The systematics on ratio are estimated by using error propogation $\sigma_{tot} = \sqrt{\sigma_a^2 + \sigma_b^2}$, where σ_a is errors on 0-40% and σ_b is errors on 40-80% centrality, as shown in figure 20 (right).

The ratio of proton-Ω correlation function from peripheral (40-80%) to central (0-40%) collisions, defined as R = C_{40-80}/C_{0-40}, for proton-Ω and anti-proton-$\bar{\Omega}$ ($P\Omega + \bar{P}\bar{\Omega}$) is shown in the upper panel of Figure 21. The systematic errors are propagated through error propagation from measured correlation function for 0-40% and 40-80% centrality and are shown as boxes. The same ratio, R, for the background is unity and is shown as open squares in the Figure 21. The predictions for the ratio of small system to large system from Ref. [11] for proton-Ω interaction potentials V_I, V_{II} and V_{III} for static source and expanding source are also shown in the Figure 21.

The bottom panel in the Figure 21 shows the absolute difference between the measurement ($R_{Measured}$) and the

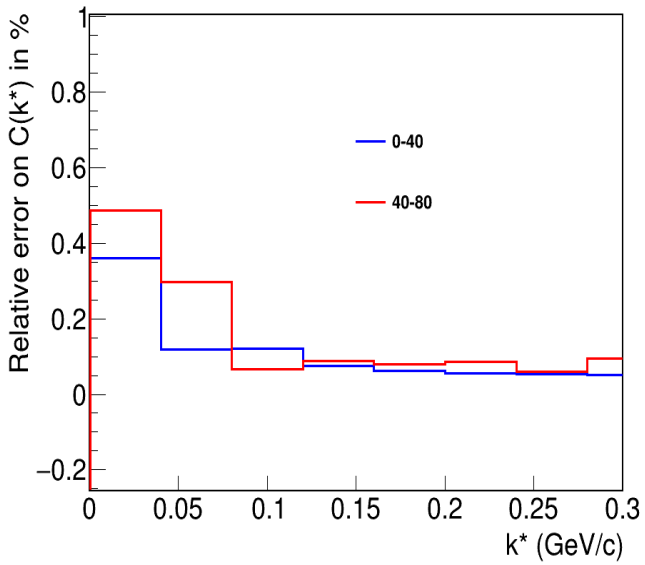

FIG. 18. Esitmated total relative errors on correlation function for 0-40% (blue) and 40-80% (red) centrality.

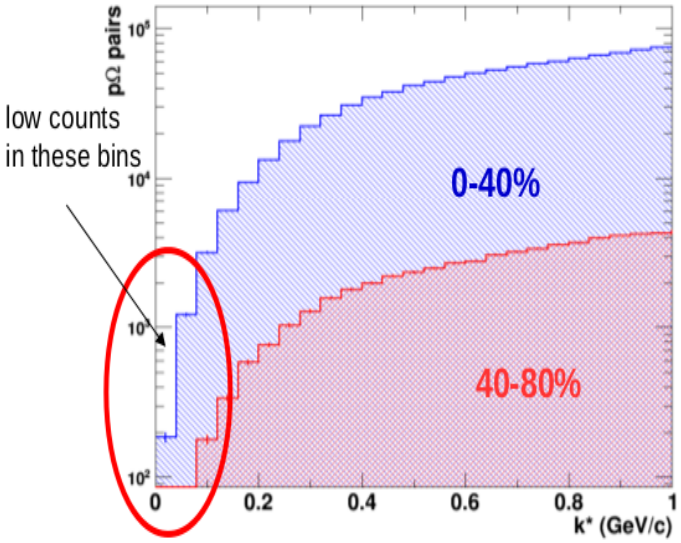

FIG. 19. Proton-Ω pairs as a function of k^* for 0-40% (blue) and 40-80% (red).

predictions (R_{Model}) divided by the error (σ). The predictions with expanding source for the proton-Ω interaction potentials V_I and V_{II} are larger than 3σ at $k^* = 20$ MeV/c. The prediction for the proton-Ω interaction potential V_{III} with expanding source and static source are close to 1σ at $k^* = 20$ MeV/c.

Comparing the measured ratio $R = 0.28 \pm 0.35_{stat} \pm 0.03_{sys}$ (background $= 0.96 \pm 0.13_{stat}$) for $k^* = 20$ MeV/c and $R = 0.81 \pm 0.22_{stat} \pm 0.08_{sys}$ (background $= 0.97 \pm 0.05_{stat}$) for $k^* = 60$ MeV/c with the Figure 5(b) from the Ref. [11], where the ratio of small system to large system at $k^* = 20$, 40 and 60 MeV/c is compared with the scattering length, we conclude that the scattering length is positive for the proton-Ω interaction. The positive scattering length and the measured ratio of proton-Ω correlation function from peripheral to central collisions less than unity for $k^* < 80$ MeV/c favors the proton-Ω interaction potential V_{III} with $E_b = 26.9$ MeV for proton-Ω.

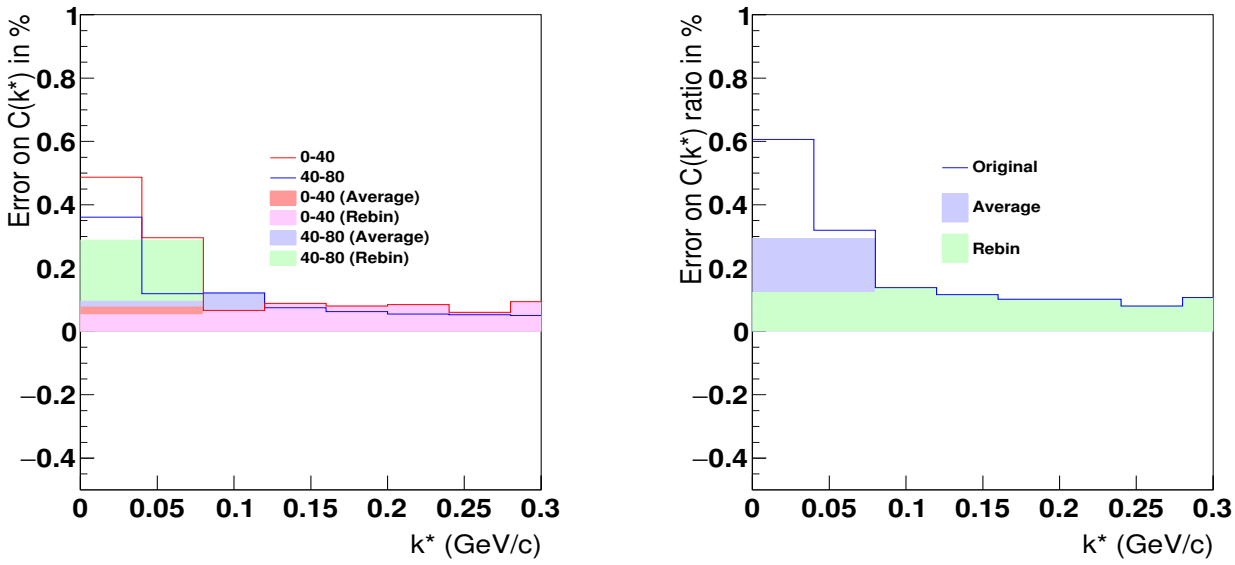

FIG. 20. On the left are esitmated relative errors on correlation function for 0-40% (blue) and 40-80% (red) centrality before rebinning (lines), after rebinning (shaded bands) and from the taking average over all the bins. On the right esitmated relative errors on the ratio of correlation function between 0-40% and 40-80% centrality from both the methods.

The proton HBT radii is 2.75 fm for the 30-80% centrality for Au+Au 200 GeV [17]. In figure 22, we show dependence of the ratio of small system to large system from [18] for proton-Ω interaction potentials V_I , V_{II} and V_{III} on source size for a static source. One can see that the ratio of small to large system becomes more sensitive to the proton-Ω interaction for smaller radii.

SUMMARY

The measured ratio of proton-Ω correlation function from peripheral to central collisions is compared with the predictions based on proton-Ω interaction extracted from (2+1)-flavor lattice QCD simulations at the physical point. The measured ratio of proton-Ω correlation function from peripheral to central collisions is less than unity for $k^* < 80$ MeV/c, which indicates that the scattering length is positive for the proton-Ω interaction and supports proton-Ω bound state hypothesis.

[1] R. Jaffe, Phys. Rev. Lett. **38**, 195 (1977).
[2] J.T. Goldman, K. Maltman, G.J. Stephenson, K.E. Schmidt and F. Wang, Phys. Rev. Lett. **59**, 627 (1987).
[3] B. Schwesinger, F.G. Scholtz and H.B. Geyer, Phys. Rev. D **51**, 1228 (1995).
[4] M. Oka, Phys. Rev. D **38**, 298 (1988).
[5] H. Pang, J. Ping, F. Wang, T. Goldmn and E. Zhao, Phys. Rev. C **69**, 065207 (2004).
[6] H. Pang, J. Ping, L. Chen, F. Wang and T. Goldmn, Phys. Rev. C **70**, 035204 (2004).
[7] M. Chen, H. Huang, J. Ping and F. Wang, Phys. Rev. C **83**, 015202 (2011).
[8] H. Huang, J. Ping and F. Wang, Phys. Rev. C **92**, 065202 (2015).
[9] Q. B. Li and P. N. Shen, Eur. Phys. J. A **8**, 417 (2002)
[10] F. Etminan *et al.* (HAL QCD Collaboration), Nucl. Phys. A **928**, 89 (2014).
[11] Kenji Morita, Akira Ohnishi, Faisal Etminan and Tetsuo Hatsuda, Phys. Rev. C **94**, 031901 (R) (2016).
[12] K. H. Ackermann *et al.* (STAR Collaboration), Nucl. Instrum. and Meth. A **499**, 624 (2003).
[13] C. Patrignani et al. (Particle Data Group), Chin. Phys. C **40**, 100001 (2016).
[14] M. Chojnacki, A. Kisiel, W. Florkowski, W. Broniowski, Comput. Phys. Commun. **183**, 746 (2012).

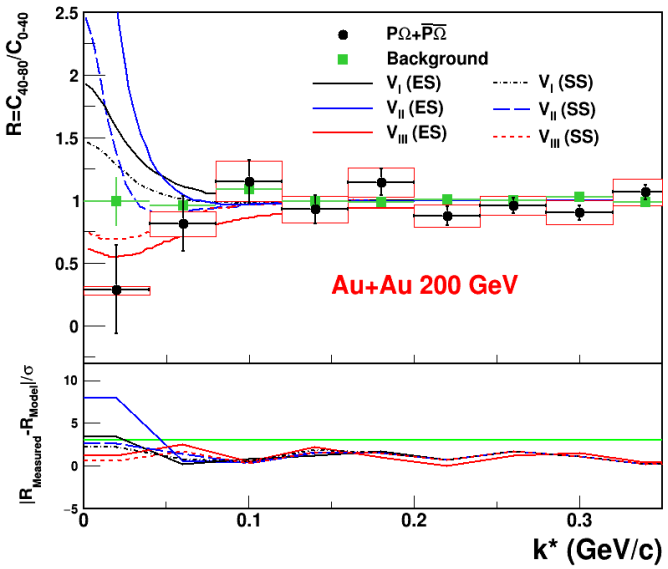

FIG. 21. (color online) The ratio (R) of small system (40-80% collisions) to large system (0-40% collisions) for proton-Ω and anti-proton-$\bar{\Omega}$ ($P\Omega + \bar{P}\bar{\Omega}$) is shown in the upper panel. The boxes correspond to the systematic error. The squares are the ratio for background candidates from the side-band of Ω invariant mass. The solid and dashed lines are prediction for the ratio of small system to large system from [11] for proton-Ω interaction potentials V_I, V_{II} and V_{III} for static source (SS) and expanding source (ES). The bottom panel shows the the absolute difference between the measurement and the predictions divided by the errors. The green line shows the 3σ.

[15] J. Adams *et al.* (STAR Collaboration), Phys. Rev. C **74**, 064906 (2006).
[16] J. Adams *et al.* (STAR Collaboration), Phys. Rev. C **71**, 044906 (2005).
[17] L. Adamczyk *et al.* (STAR Collaboration), Nature 527 (2015) 345.
[18] Private communications with Kenji Morita, Akira Ohnishi.

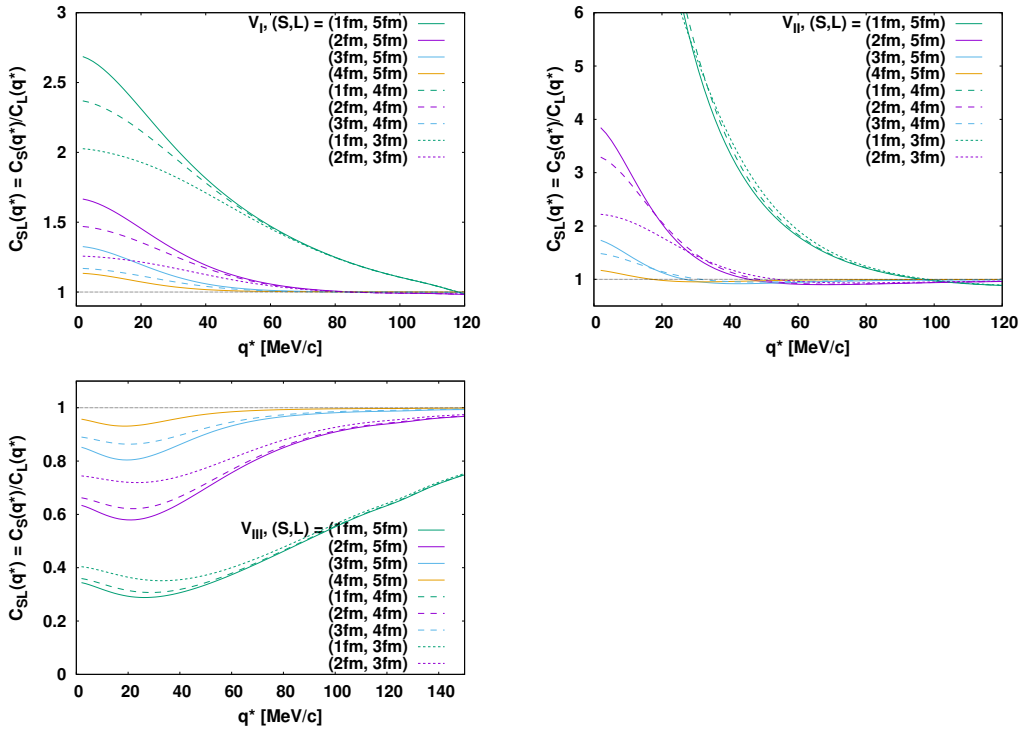

FIG. 22. Predictions for the ratio of small system to large system from [18] for proton-Ω interaction potentials V_I , V_{II} and V_{III} for static source with different source sizes S and L corresponding to small and large systems.